Block-Median Pyramidal Transform: Analysis and Denoising Applications

Vladimir P. Melnik, Ilya Shmulevich, *Member, IEEE*, Karen Egiazarian, *Senior Member, IEEE*, and Jaakko Astola, *Fellow, IEEE*

***Abstract*—A nonlinear multiscale pyramidal transform based on nonoverlapping block decompositions using the median operation and a polynomial approximation is considered. It is shown that this structure can be useful for denoising of one– and two-dimensional (1-D and 2-D) signals. Various denoising techniques are analyzed, including methods based on spatially adaptive thresholding and partial cycle-spinning algorithms. An analytical method for deriving the distribution function of the transform coefficients is also presented. This, in turn, can be used for the selection of thresholds for denoising applications.**

***Index Terms*—Denoising, multiresolution, nonlinear filter, pyramidal transform.**

I. Introduction

In recent years, multiscale techniques have been popular in many signal and image processing applications. Some directions in this field have focused on pyramidal transforms [1]–[6]. A number of applications based on such transforms have been proposed in compression [3], [7], coding [1], [8], [9]–[11], and denoising [5], [6], [12]–[14].

In the pyramidal decomposition scheme, a signal is successively decomposed into a decimated "lowpass" version and a signal containing residual information [1], [5]. This residual signal is computed as a difference between the signal on a finer scale and the interpolated signal from a coarser scale. An important distinguishing feature of such a scheme is its overcompleteness, which means that the size of the transform coefficients is larger than the size of the initial signal. The framework of pyramidal decomposition allows the construction of multiresolution structures based on a variety of nonlinear operations, resulting in a rich set of efficient tools for many applications.

For example, in [2] and [5], the techniques of design of morphological pyramids are described. In [3], the distance order-statistic filter is used as a basis for the pyramidal transform. In [5] and [7], the pyramidal median transform (PMT) is proposed with applications to astronomical image processing. Another example of a pyramid using the median operation is the median-interpolating pyramid transform (MIPT) [6], [15]. It not only utilizes median filtering but also makes use of a nonlinear interpolation based on median imputation [6]. Multiscale structures can be based on critically sampled nonlinear multiresolution schemes. For example, one such scheme is proposed in [16].

In this paper, we consider a block-median pyramidal transform based on a nonoverlapping block decomposition and polynomial interpolation [17]. For this transform, the median filter used at the decomposition stage is applied to nonoverlapping blocks only. The outputs of the median operation, applied iteratively, constitute the signals at consecutive scale levels.

One direction of our work deals with the application of pyramidal transforms for noise removal. Techniques of pyramidal denoising are similar to those in wavelet-based methods. In order to remove noise, they use the thresholding of transform coefficients [5], [6]. For wavelet techniques, this field of application is well studied. At the same time, pyramidal techniques, being less popular than their wavelet counterparts, require more detailed investigation and analysis.

For example, an important problem connected with the applications of pyramidal transforms is the analysis of statistical properties of the transform coefficients [6]. For the block-median pyramidal transform, we present an analytical method for deriving the probability distribution of transform coefficients. This, in turn, permits us to make an appropriate choice of threshold values for denoising.

In addition to hard and soft thresholding, we also consider other denoising techniques based on partial cycle-spinning algorithms and local adaptation. Cycle-spinning algorithms provide a shift-invariance property of multiscale transforms and are successfully used for wavelet denoising [18]. The proposed local adaptation permits different treatment of details and homogeneous regions of the image in the pyramidal transform domain.

In Section II, we give a detailed description of the block-median pyramidal transform (BMPT). Section III is devoted to the analysis of statistical properties of transform coefficients. Finally, the methods of denoising using pyramidal transforms are analyzed in Section IV.

II. Block-Median Pyramidal Transform

A general structure of pyramidal transforms, consisting of decomposition and reconstruction stages, is depicted in Fig. 1 for two levels of decomposition. It is seen from Fig. 1 that the filter operator is applied to signal $x^{(k)}(i)$ on some scale level k followed by downsampling by M. This constitutes the shrunk signal $x^{(k+1)}(i)$ at the next, coarser scale $k+1$. Clearly, the size of the signal on each successive scale is reduced by M. Afterwards, upsampling by M and the interpolation operator are used to predict the data on scale k from scale $k+1$. The dif-

Manuscript received August 16, 1999; revised October 24, 2000. The associate editor coordinating the review of this paper and approving it for publication was Dr. Kenneth Kreutz-Delgado.

The authors are with the Signal Processing Laboratory, Tampere University of Technology, Tampere, Finland.

Publisher Item Identifier S 1053-587X(01)00637-7.

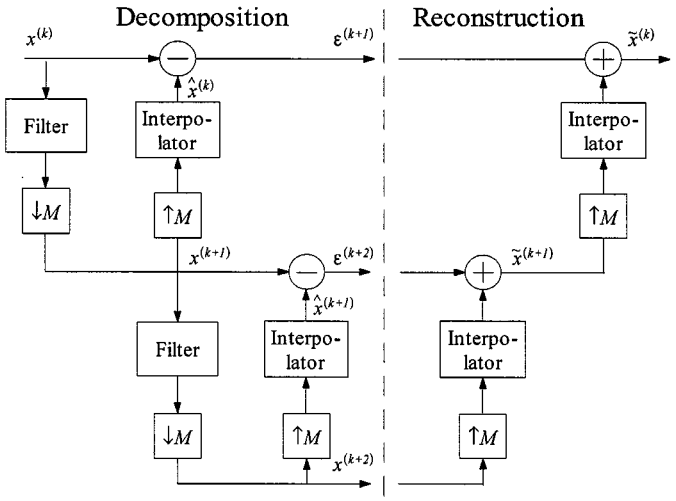

Fig. 1. General stucture of a pyramid transform.

ferences between the actual and predicted values are calculated and stored as the residual signal $\varepsilon^{(k+1)}(i)$. Further decomposition is achieved by iterating this process.

The described structure generalizes the majority of well-known pyramidal transforms with perfect reconstruction ability, such as the Laplacian pyramid [1] and the PMT [5]. The Laplacian pyramid proposed for image processing uses a linear FIR filter with appropriate weights both as the filter operator and the interpolator. In that case, the downsampling/upsampling factor M is equal to 4, i.e., the horizontal and vertical image dimensions are reduced twofold from finer scales to coarser scales. The PMT is a nonlinear pyramidal transform that uses the median filter as the filter operator and splines as interpolators. The PMT was proposed for the 2-D case with $M = 4$.

However, some pyramids cannot be represented in such a way as in Fig. 1. For example, in the iterative median pyramid transform [4], the signal at the output of the median filter, before downsampling, is used as the prediction from coarser to finer scales. Thus, perfect reconstruction is not possible in this case. In the MIPT [6], the initial signal $x^{(0)}(i)$ is needed in order to obtain the shrunk signal at each scale level. More precisely, the signal at each scale is obtained by using the median operation over nonoverlapping blocks of $x^{(0)}(i)$. Clearly, the size of these blocks increases with each scale level. The interpolator for the MIPT is based on a nonlinear procedure called median imputation. However, as mentioned in [15], this interpolation can be well approximated by linear Lagrange interpolation. The MIPT has a triadic structure, which means that for 1-D signals, the downsampling/upsampling factor M is equal to 3.

Below, we consider the BMPT based on nonoverlapping blocks of the data. In contrast to the MIPT, it can be represented using the general structure in Fig. 1. Algorithms 1 and 2 describe the decomposition and reconstruction parts of this transform. The BMPT lends itself to fast implementation. There is no need to calculate the filter outputs for the entire signal and then decimate it. Instead, one can collect only the outputs of the filter applied to nonoverlapping blocks of the signal.

Algorithm 1: BMPT Decomposition

1) Let $x^{(k)}(i)$ represent the signal on scale level k. Start with $k = 0$, which is the original signal $x(i)$ of size M^n.
2) Divide $x^{(k)}(i)$ into nonoverlapping blocks of size M.
3) The signal $x^{(k+1)}(i)$ on scale $k+1$ is obtained by applying the median operator to each nonoverlapping block of $x^{(k)}(i)$.
4) Interpolate $x^{(k+1)}(i)$ to make the prediction $\hat{x}^{(k)}(i)$ of the signal on scale k.
5) Compute and store the differences $\varepsilon^{(k+1)}(i) = x^{(k)}(i) - \hat{x}^{(k)}(i)$.
6) Let $k = k+1$. If $k < K_0$ ($K_0 \leq n$), go to 2.
7) Collect the set of transform coefficients, where $\mu = \{\varepsilon^{(1)}(i), \cdots, \varepsilon^{(K_0)}(i), x^{(K_0)}(i)\}$.

Algorithm 2: BMPT Reconstruction

1) Let $k = K_0$.
2) Interpolate $x^{(k)}(i)$ to make the prediction $\hat{x}^{(k-1)}(i)$ of the signal on scale $k-1$.
3) The signal on scale $k-1$ is obtained by $x^{(k-1)}(i) = \varepsilon^{(k)}(i) + \hat{x}^{(k-1)}(i)$.
4) Let $k = k-1$. If $k > 0$, go to 2.
5) Let $x(i) = x^{(0)}(i)$.

The size N_μ of transform coefficients for the BMPT as well as for the general pyramidal transform depicted in Fig. 1 depends on the factor M and the number of decomposition levels K_0. If the size of the initial signal $x(i)$ is equal to M^n, then we have

$$N_\mu = M^{n-K_0} + M^{n-K_0+1} + \cdots + M^n = \frac{M^{n+1} - M^{n-K_0}}{M-1}. \tag{1}$$

Small decimation rates permit one to decompose the signal into a larger number of resolution levels. Consequently, it leads to more accurate separation of the signal details from scale to scale. On the other hand, larger downsampling/upsampling rates lead to a decrease in the transform size for a given signal of prescribed length. For example, when $M = 3$ and the length of the initial signal is $N_x = 3^n$, then $N_\mu \sim 3/2N_x$ when K_0 is large. At the same time, for $M = 2$ and $N_x = 2^n$, we have $N_\mu \sim 2N_x$, indicating a larger size of transform coefficients with respect to the initial signal length. This is one reason we favor the use of large decimation rates [9]. Overcompleteness of pyramidal transforms, being a problem for coding, has little or no impact in denoising applications. Moreover, one could use "nondownsampled" multiscale transforms such as those proposed in [5] and [19].

Let us first consider the BMPT for the 1-D case when $M = 3$. The shrunk signal at scale $k+1$ is obtained by using the median operation over triadic blocks of the signal $x^{(k)}(i)$ on scale k. Analytically, it can be expressed as

$$x^{(k+1)}(i) = \text{med}\,[x^{(k)}(3i-2), x^{(k)}(3i-1), x^{(k)}(3i)] \tag{2}$$

where $i = 1, \cdots, 3^{n-k-1}$. For the purpose of defining the interpolating polynomial and without loss of generality, we may define an arbitrary time axis. For simplicity, let us associate time $t = 0$ with $x^{(k+1)}(i)$ and times $t = -1, 1$ with $x^{(k+1)}(i-1)$

and $x^{(k+1)}(i+1)$, respectively. Consider a second-order polynomial

$$p(t) = at^2 + bt + c$$

which passes through points $x^{(k+1)}(i-1), x^{(k+1)}(i)$, $x^{(k+1)}(i+1)$. Using this polynomial, we make a prediction of the points $\hat{x}^{(k)}(3i-2)$, $\hat{x}^{(k)}(3i-1)$, and $\hat{x}^{(k)}(3i)$ on level k. Specifically

$$\begin{aligned}\hat{x}^{(k)}(3i-2) &= p(-\tfrac{1}{3}) \\ \hat{x}^{(k)}(3i-1) &= p(0) \\ \hat{x}^{(k)}(3i) &= p(\tfrac{1}{3}).\end{aligned}$$

After solving for the coefficients of $p(t)$, the interpolator makes the prediction from scale $k+1$ to the kth scale as follows:

$$\begin{aligned}\hat{x}^{(k)}(3i) = &-\tfrac{1}{9}x^{(k+1)}(i-1) + \tfrac{8}{9}x^{(k+1)}(i) \\ &+ \tfrac{2}{9}x^{(k+1)}(i+1) \qquad (3a)\\ \hat{x}^{(k)}(3i-1) = &\, x^{(k+1)}(i) \qquad (3b)\\ \hat{x}^{(k)}(3i-2) = &\, \tfrac{2}{9}x^{(k+1)}(i-1) + \tfrac{8}{9}x^{(k+1)}(i) \\ &- \tfrac{1}{9}x^{(k+1)}(i+1) \qquad (3c)\end{aligned}$$

where $i = 2, \cdots, 3^{n-k-1} - 1$. Formulas (3a)–(3c) can be rewritten in a general expression, depending on the parameters $\alpha_{-1}(l), \alpha_0(l), \alpha_1(l)$ as

$$\begin{aligned}\hat{x}^{(k)}(3i-l) = &\, \alpha_{-1}(l)x^{(k+1)}(i-1) \\ &+ \alpha_0(l)x^{(k+1)}(i) + \alpha_1(l)x^{(k+1)}(i+1) \qquad (4)\end{aligned}$$

where $i = 2, \cdots, 3^{n-k-1} - 1$ and $l = 0, 1, 2$. Fig. 2 illustrates the above relationships between shrunk signals at scale levels k and $k+1$ as well as residual signal values and polynomial interpolation.

The border effects are not accounted for in (3a)–(3c) and (4). For example, one can assume

$$\begin{aligned}(\hat{x}^{(k)}(i))_{i=1,2,3} &= x^{(k+1)}(1) \quad \text{and} \\ (\hat{x}^{(k)}(3^{n-k} - l))_{l=0,1,2} &= x^{(k+1)}(3^{n-k-1}).\end{aligned}$$

An example of the decomposition of the "Doppler" signal using the BMPT is presented in Fig. 3.

The BMPT can easily be adapted for image processing applications [20] by applying the median operation to 2-D nonoverlapping blocks of size M and using Lagrange interpolation [21]. Let $x(i,j)$ be the 2-D signal of size $N \times N, N = M^{n/2}$. For example, if $M = 9$, the shrunk signal on scale $k+1$ can be written as

$$x^{(k+1)}(i,j) = \text{med}\,[x^{(k)}(3i-l, 3j-r)]_{l,r=0,1,2} \qquad (5)$$

where $i, j = 1, \cdots, 3^{n-k-1}$. In this case, the interpolation operator from scale $k+1$ to scale k can be represented generally by

$$\begin{aligned}&\hat{x}^{(k)}(3i-l, 3j-r) \\ &\quad = \sum_{p=-1}^{1}\sum_{q=-1}^{1} \alpha_{pq}(l,r)x^{(k+1)}(i+p, j+q) \qquad (6)\end{aligned}$$

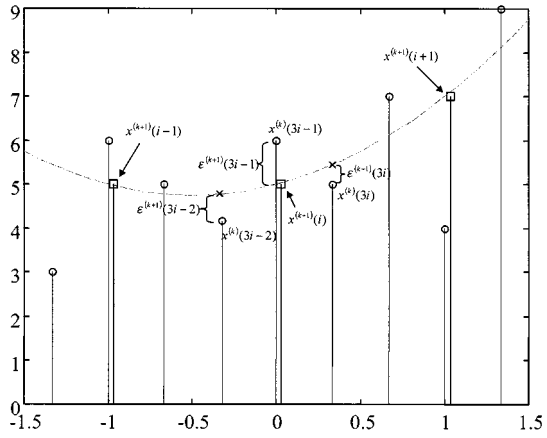

Fig. 2. Relationships between two consecutive shrunk signals. Shrunk signal values at scale k (circles); shrunk signal values at scale $k+1$ (squares); prediction values from scale $k+1$ to scale k (crosses); polynomial interpolation (dashed line).

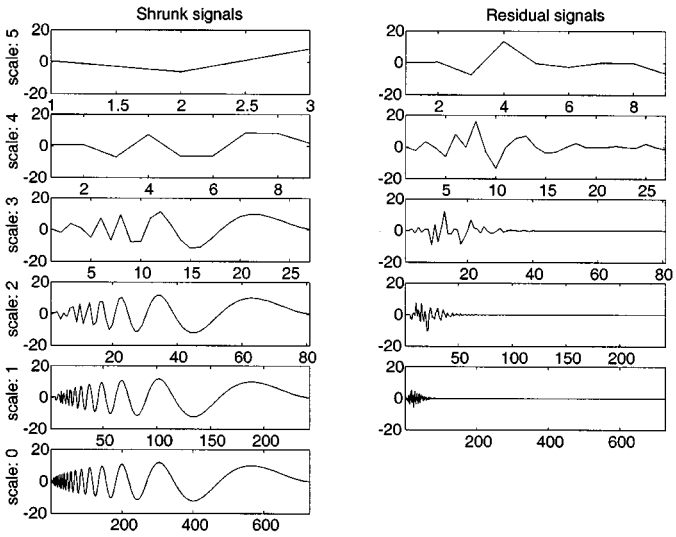

Fig. 3. "Doppler" signal decomposition using BMPT.

where $i, j = 2, \cdots, 3^{n-k-1} - 1$, $l, r = 0, 1, 2$, and α_{pq} are the parameters calculated beforehand using the Lagrange interpolation formula [21].

III. Probability Distribution of Transform Coefficients of BMPT

Ultimately, the BMPT is intended for noise reduction. In order for us to understand the BMPTs ability to suppress noise, we must analyze the statistical characteristics of the decomposition of the noise itself, which is assumed to be comprised of i.i.d. random variables. We stress, however, that such an assumption in no way implies any restrictions on the model of the uncorrupted signal.

In this section, we describe a procedure for analytically determining the probability distribution of the transform coefficients of the BMPT. Because of the above considerations, the input to the BMPT is modeled as a sequence of i.i.d. random variables $x(i)$ with distribution $F_{x^{(0)}}(x)$. The cumulative distribution function (cdf) of the shrunk signal at each scale level k can

be easily derived from the distribution function of the signal on scale level $k-1$ by using the formula [22, p. 65]

$$F_{x^{(k)}}(t) = 3F^2_{x^{(k-1)}}(t) - 2F^3_{x^{(k-1)}}(t). \tag{7}$$

Our goal is to compute the cdf $F_{\varepsilon^{(k)}}(t) = \Pr\{\varepsilon^{(k)} \le t\}$ of the residual signal $\varepsilon^{(k)}(i)$ on each scale level k. Using the general interpolator in (4), we can express $\varepsilon^{(k)}(i)$ as

$$\begin{aligned}\varepsilon^{(k)}(3i-l) &= x^{(k)}(3i-l) - \hat{x}^{(k)}(3i-l)\\ &= x^{(k)}(3i-l) - \alpha_{-1}(l)x^{(k+1)}(i-1)\\ &\quad - \alpha_0(l)x^{(k+1)}(i)\\ &\quad - \alpha_1(l)x^{(k+1)}(i+1)\\ &= z(i,l) + w(i,l) + v(i,l)\end{aligned} \tag{8}$$

where $i = 2, \cdots, 3^{n-k-1}-1$, parameter $l = 0,1,2$, and

$$\begin{aligned}z(i,l) &= x^{(k)}(3i-l) - \alpha_0(l)x^{(k+1)}(i)\\ w(i,l) &= -\alpha_{-1}(l)x^{(k+1)}(i-1)\\ v(i,l) &= -\alpha_1(l)x^{(k+1)}(i+1).\end{aligned}$$

To make the above relationships more clear, see Fig. 2. The nonoverlapping nature of this pyramidal transform ensures us that the shrunk signals on each scale level will consist of i.i.d. random variables. It is clear that $z(i,l), w(i,l)$, and $v(i,l)$ are independent random variables for any given i.

Let us begin by deriving the probability density functions $f_w(t;l)$ and $f_v(t;l)$ of random variables $w(i,l)$ and $v(i,l)$. These densities are obtained by a simple linear transformation from random variable $x^{(k+1)}(i)$ and are found to be

$$\begin{aligned}f_w(t;l) &= [\alpha_{-1}(l)]^{-1} f_{x^{(k+1)}}(-t/\alpha_{-1}(l))\\ f_v(t;l) &= [\alpha_1(l)]^{-1} f_{x^{(k+1)}}(-t/\alpha_1(l))\end{aligned}$$

where $f_{x^{(k)}}(t) = (\partial/\partial t)F_{x^{(k)}}(t)$.

The next step is to calculate the pdf of random variable $z(i,l)$ by introducing an auxiliary variable $\xi = x^{(k+1)}(i)$

$$f_z(t;l) = \int_{-\infty}^{\infty} f_{x^{(k)},x^{(k+1)}}(t + \alpha_0(l)\xi, \xi)\, d\xi. \tag{9}$$

This involves the calculation of the joint density $f_{x^{(k)},x^{(k+1)}}(t_1,t_2;l)$ between random variables $x^{(k)}(3i-l)$ and $x^{(k+1)}(i)$ for $l = 0,1,2$. In other words, this is the joint density between two corresponding shrunk signal values on consecutive scale levels k and $k+1$. Note that the Jacobian of the transformation from $x^{(k)}(3i-l), x^{(k+1)}(i)$ to $z(i,l), \xi$ is equal to 1. We begin by expressing $x^{(k)}(3i-l)$ and $x^{(k+1)}(i)$ as outputs of different stack filters $S_1^{(l)}(\cdot)$ and $S_2(\cdot)$ with the same inputs [23]. Specifically, $S_1^{(l)}(\cdot)$ are three identity filters for $l = 0,1,2$, and $S_2(\cdot)$ is the median filter

$$\begin{aligned}&S_1^{(l)}(x^{(k)}(3i-2), x^{(k)}(3i-1), x^{(k)}(3i))\\ &\quad = x^{(k)}(3i-l),\ l = 0,1,2\\ &S_2(x^{(k)}(3i-2), x^{(k)}(3i-1), x^{(k)}(3i))\\ &\quad = \text{med}\,[x^{(k)}(3i-2), x^{(k)}(3i-1), x^{(k)}(3i)].\end{aligned}$$

In order to compute $f_{x^{(k)},x^{(k+1)}}(t_1,t_2;l)$, we use the well-known formula for the joint distribution of the outputs of two stack filters having i.i.d. inputs with distribution $F(t)$ [24]:

$$\begin{aligned}\Psi(t_1,t_2) = \sum_{i=0}^{M}\sum_{j=0}^{M} A_{ij}F^i(t_1)(F(t_2)\\ - F(t_1))^{M-i-j}(1-F(t_2))^j\end{aligned} \tag{10}$$

where

$$\begin{aligned}A_{ij} = |\{a,b \in \{0,1\}^M; a \ge b,\, g(a) = h(b) = 0\\ \rho(\overline{a} \circ \overline{b}) = i, \rho(a \circ b) = j\}|\end{aligned}$$

and

$\rho(c)$	Hamming weight of c;
$\overline{a}$	complement of a;
$a \circ b$	pointwise product of a and b;
M	window width of the stack filters, which is equal to the block size.

In this case, $M = 3$. By direct application of (10), we find that the joint cdf of $x^{(k)}(3i-l)$ and $x^{(k+1)}(i)$ is equal to

$$F_{x^{(k)},x^{(k+1)}}(t_1,t_2) = F^2_{x^{(k)}}(t_1)[F_{x^{(k)}}(t_2) - 2F_{x^{(k)}}(t_1) + 2]$$

and the joint pdf becomes

$$\begin{aligned}&f_{x^{(k)},x^{(k+1)}}(t_1,t_2)\\ &\quad = \frac{\partial^2 F_{x^{(k)},x^{(k+1)}}(t_1,t_2)}{\partial t_1 \partial t_2}\\ &\quad = 2F_{x^{(k)}}(t_1)\frac{\partial F_{x^{(k)}}(t_1)}{\partial t_1}\,\frac{\partial F_{x^{(k+1)}}(t_2)}{\partial t_2}\\ &\quad = 12F_{x^{(k)}}(t_1)F_{x^{(k)}}(t_2)\frac{\partial F_{x^{(k)}}(t_1)}{\partial t_1}\\ &\qquad \cdot \frac{\partial F_{x^{(k)}}(t_2)}{\partial t_2}(1 - F_{x^{(k)}}(t_2))\end{aligned} \tag{11}$$

where the last equality in (11) is obtained by using (7). Note that the obtained joint distribution $F_{x^{(k)},x^{(k+1)}}(t_1,t_2)$ does not depend on l. To obtain $f_z(t;l)$, we substitute (11) into (9).

Finally, the pdf of the values of the residual signal $\varepsilon^{(k)}(i)$ on each scale level k can be obtained by convolving the densities of $z(i,l), w(i,l)$, and $v(i,l)$ since they are independent.

$$f_{\varepsilon^{(k)}}(t;l) = f_z(t;l) * f_w(t;l) * f_v(t;l).$$

The cumulative distribution is then

$$F_{\varepsilon^{(k)}}(t;l) = \int_{-\infty}^{t} f_{\varepsilon^{(k)}}(\omega;l)\, d\omega.$$

As an example, Fig. 4 shows the pdfs of the input signal $x^{(0)}(i)$, which is Normal (0,1), of the shrunk signal $x^{(1)}(i)$ and of the residual signal $\varepsilon^{(1)}(i)$.

IV. Denoising Applications of BMPT

A. Thresholding of Transform Coefficients

As in many other multiresolution techniques, the algorithms of pyramidal denoising are based on a thresholding procedure

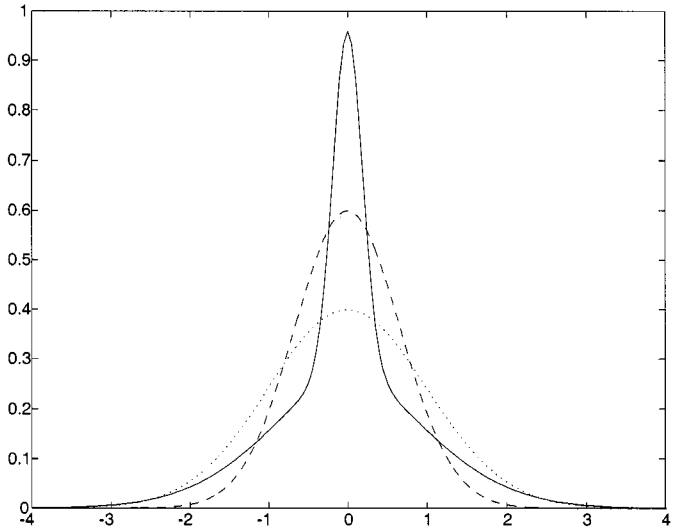

Fig. 4. The pdfs $f_{x^{(0)}}(t) \sim N(0,1)$ (dotted line), $f_{x^{(1)}}(t)$ (dashed line), and $f_{\varepsilon^{(1)}}(t)$ (solid line).

of the transform coefficients. Generally, the denoising algorithm has the following three steps.

1) Obtain the set $\mu = \{\varepsilon^{(1)}(i), \cdots, \varepsilon^{(K_0)}(i), x^{(K_0)}(i)\}$ by applying the pyramidal decomposition algorithm to noisy data.
2) Apply a thresholding operator $\eta[\cdot]$ to the residual signal values $\{\varepsilon^{(1)}(i), \cdots, \varepsilon^{(K_0)}(i)\}$.
3) Invert the pyramidal transform by applying the pyramidal reconstruction algorithm to the set of thresholded coefficients $\mu_t = \{\eta[\varepsilon^{(1)}(i)], \cdots, \eta[\varepsilon^{(K_0)}(i)], x^{(K_0)}(i)\}$.

The simplest and the most widely used thresholding operators make use of the so-called hard and soft thresholding schemes [6], [25]. The hard thresholding scheme can be described by the function

$$\eta_{\text{hard}}(\varepsilon^{(k)}(i); t_k) = \begin{cases} \varepsilon^{(k)}(i), & |\varepsilon^{(k)}(i)| > t_k \\ 0, & |\varepsilon^{(k)}(i)| \le t_k \end{cases} \tag{12}$$

where t_k is a fixed threshold on scale k. The hard thresholding procedure assumes that the transform coefficients with amplitudes smaller than t_k can be considered as the ones corresponding to noise and, hence, can be set to zero. The threshold t_k controls the degree of noise reduction.

The soft thresholding operator is expressed as a function depending on the threshold t_k in the following way:

$$\eta_{\text{soft}}(\varepsilon^{(k)}(i); t_k) = \begin{cases} \text{sign}(\varepsilon^{(k)}(i))(|\varepsilon^{(k)}(i)| - t_k), & |\varepsilon^{(k)}(i)| > t_k \\ 0, & |\varepsilon^{(k)}(i)| \le t_k. \end{cases} \tag{13}$$

In [25], it is shown that wavelet denoising based on the soft thresholding scheme obtains a near optimal recovery of noisy data for a wide range of smoothness classes. A method of choosing a fixed threshold based on the standard deviation of noise is also proposed.

One approach to threshold selection is to make use of statistical characteristics of the transform coefficients corresponding to the pure noise input signal [15], [25]. The noise is assumed to be white and additive. In particular, we can choose the "hard" threshold t_k, $1 \le k \le K_0$ on each scale level so that the probability of the transform coefficients $|\varepsilon^{(k)}(i)|$ exceeding it is at most equal to some probability p for the case of $x(i)$ being white noise with some given probability distribution [6], that is

$$\Pr\{|\varepsilon^{(k)}(i)| > t_k\} = p. \tag{14}$$

The soft and hard thresholding schemes can be applied for denoising using the introduced block-median pyramidal transform. Moreover, the statistical results obtained in Section III give the possibility of analytically determining the "hard" and "soft" thresholds for the BMPT. Rewriting (14) using the distribution $F_{\varepsilon^{(k)}}(t; l)$ of the residual signal values on scale k, we obtain

$$p = 1 - F_{\varepsilon^{(k)}}(t_k; l) + F_{\varepsilon^{(k)}}(-t_k; l). \tag{15}$$

Now, one can derive the "hard" thresholds t_k, $k = 1, \cdots, K_0$ by solving (15) using the technique described in Section III for calculating the distribution $F_{\varepsilon^{(k)}}(t; l)$.

Another possibility is to select the thresholds by estimating the standard deviation $\sigma^{(k)}$ of the noise at each scale [7]. The "hard" thresholds in this case are calculated as $t_k = \gamma\sigma^{(k)}$, where γ is a parameter, which is typically between 2 and 4. The "soft" thresholds can also be set, depending on $\sigma^{(k)}$. In particular, for the BMPT, we propose to set the thresholds close to the value $\sigma^{(k)}$, i.e., $t_k \approx \sigma^{(k)}$. Therefore, we have to evaluate the values of the standard deviation $\sigma^{(k)}$ on each scale level. For the BMPT, it can be done using the expression

$$\sigma^{(k)} = \sqrt{\int_{-\infty}^{\infty} u^2 dF_{\varepsilon^{(k)}}(u; l) - \left(\int_{-\infty}^{\infty} u dF_{\varepsilon^{(k)}}(u; l)\right)^2}.$$

B. Spatially Adaptive and Hybrid Denoising Techniques

The considered hard and soft thresholding schemes are effective in many situations. However, adaptive thresholding rules can significantly improve the efficiency of denoising. They permit one to adapt to both noise and signal characteristics. One way to build an algorithm based on such rules is to vary the characteristics of the thresholding operator in accordance with the value of an adaptation parameter calculated for every location at each scale level. Many well-known spatially adaptive denoising techniques can be represented in this context. The adaptation in multiscale transform domain is often based on either the derivation of local statistics of the signal in the transform domain [14], [26]–[28] or the application of multiscale edge detector operators [29].

We propose to calculate the values of a local activity indicator (LAI) at each location on each scale. The LAI reflects a spatial variability of a signal. In other words, the larger the value of the LAI, the more details are present in the signal at a given location. Local statistics, such as the local variance, can be used as the LAI.

Let us introduce the scale dependent LAI for 1-D signal $x(i)$ based on the local variance and the BMPT with downsampling by 3 as

$$v^{(k)}(i) = \frac{1}{L}\sum_{j=-L_0}^{L_0}(x^{(k-1)}(i+j))^2 - \left[\frac{1}{L}\sum_{j=-L_0}^{L_0}x^{(k-1)}(i+j)\right]^2 \quad (16)$$

where $i = 1, \cdots, 3^{n-k+1}$ and $L = 2L_0 + 1$ is the window size for local variance calculation. In other words, the values $v^{(k)}(i)$ on scale k represent the local variance calculated over the shrunk signal $x^{(k-1)}$ on the previous scale $k-1$. The size of the signal $v^{(k)}(i)$ and the residual signal $\varepsilon^{(k)}(i)$ coincide. At this point, the BMPT-based adaptive denoising can use a thresholding operation with spatially varying thresholds, depending on the values $v^{(k)}(i)$. In particular, a simple adaptive thresholding is obtained by the function

$$\eta_{\text{ad}}(\varepsilon^{(k)}(i); v^{(k)}(i); t_k) = \begin{cases} \varepsilon^{(k)}(i), & v^{(k)}(i) > t_k \\ 0, & v^{(k)}(i) \le t_k \end{cases} \quad (17)$$

where t_k is the threshold parameter. It is demonstrated in Section IV-D that this thresholding procedure is effective when applying BMPT-based denoising.

Finally, it should be mentioned that different thresholding schemes can be combined together into a hybrid structure. For example, there exist wavelet-based and locally adaptive transform-based algorithms, which result in improvement of the detail preservation as well as robustness to outliers [30].

C. Translation Invariance

It is worth noting that the pyramidal transforms considered above, like many other multiresolution decompositions, are not translation invariant. This means that the errors after denoising will be sensitive to the positions of discontinuities in the data. In order to avoid such effects, it is necessary to build translation-invariant versions of these transforms. For example, in [18] and [31], the time-invariant schemes of wavelet-based decompositions have been proposed and have been often referred to as cycle spinning. These schemes were shown to be effective tools for denoising. That suggested to us the use of similar methods for BMPT-based denoising as well.

The translation-invariant version of the pyramidal decomposition can be based on a procedure that performs all possible cyclic shifts of the initial signal and stores the transform coefficients of each shifted signal. Obviously, this leads to a redundant representation of the signal. In particular, the number of different representations equals M^{K_0}, depending on the downsampling factor M and the number of scale levels K_0. When the translation-invariant decomposition is used for denoising, it is necessary to apply the thresholding procedure to all the transform coefficients and then to reconstruct the signal from the set of representations. There are several reconstruction techniques that, for instance, can make use of averaging or median operations [18]. The efficiency of a particular technique is determined by signal and noise characteristics.

One drawback of the translation-invariant pyramidal decomposition is the large size of the set of transform coefficients and, consequently, a large number of computations in comparison with the translation-noninvariant transform. Therefore, it is reasonable to consider a partial cycle-spinning (PCS) algorithm. In the PCS, only some of all possible cyclic shifts are performed while obtaining the transform coefficients. The number of decompositions in the PCS will be referred to as $N_{\text{part}} \le M^{K_0}$. This approach is based on the assumption that the discontinuities are more likely to be found on finer scales of the pyramid.

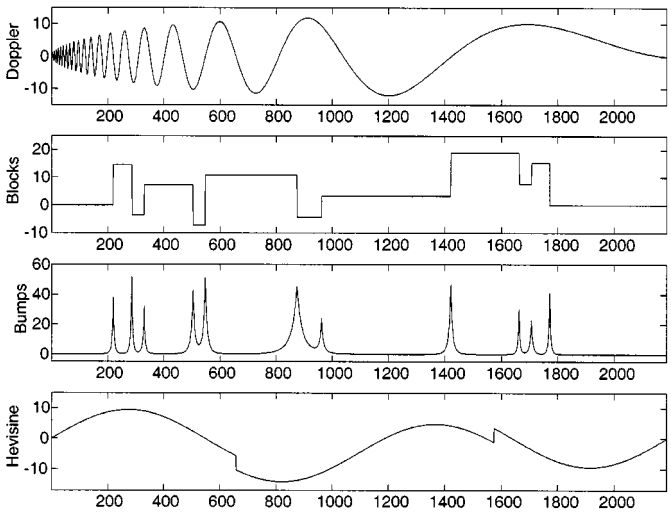

Fig. 5. One-dimensional test signals.

TABLE I
RESULTS OF NUMERICAL SIMULATIONS FOR GAUSSIAN NOISE ($\sigma = 3$)

	"Doppler"		"Blocks"		"Bumps"		"Hevisine"	
	SNR,dB	MAE	SNR,dB	MAE	SNR,dB	MAE	SNR,dB	MAE
Noisy	7.3	2.43	9.4	2.43	7.9	2.43	7.5	2.43
Wavelet	16.7	0.66	15.6	0.94	13.4	1.00	21.4	0.39
BMPT	14.1	1.00	16.5	0.92	13.4	1.00	17.2	0.73
MIPT	13.1	1.14	15.4	0.95	12.0	1.15	18.3	0.69
PMT	14.1	0.96	17.2	0.79	12.2	1.08	20.1	0.54

TABLE II
RESULTS OF NUMERICAL SIMULATIONS FOR LAPLACIAN NOISE ($\sigma = 3$)

	"Doppler"		"Blocks"		"Bumps"		"Hevisine"	
	SNR,dB	MAE	SNR,dB	MAE	SNR,dB	MAE	SNR,dB	MAE
Noisy	4.5	3.01	6.6	3.01	5.1	3.01	4.7	3.01
Wavelet	14.3	0.97	13.2	1.28	10.5	1.49	18.7	0.63
BMPT	13.6	0.97	15.0	0.95	10.0	1.22	18.9	0.62
MIPT	12.4	1.19	14.2	0.95	8.9	1.33	19.0	0.63
PMT	14.0	0.92	16.3	0.77	9.4	1.14	21.2	0.49

D. Numerical Simulations

In order to test the BMPT, we have performed numerical simulations for several test signals. Signals "Doppler," "Blocks," "Hevisine," and "Bumps" were used for the 1-D case and are depicted in Fig. 5. The mean absolute error (MAE) and SNR

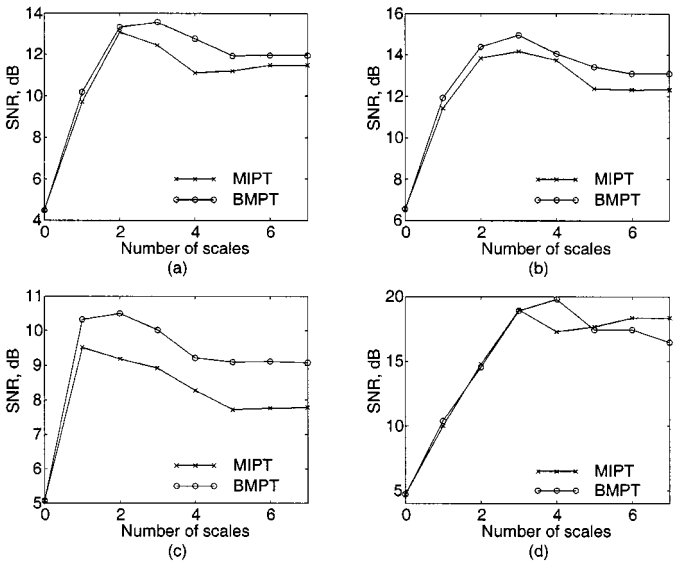

Fig. 6. Dependencies of the SNR values versus the number of scales K_0 for 1-D test signals. (a) "Doppler." (b) "Blocks." (c) "Bumps." (d) "Hevisine."

TABLE III
DENOISING USING BMPT WITH PCS FOR THE "BLOCKS" SIGNAL CORRUPTED BY GAUSSIAN NOISE ($\sigma = 3$)

Reconstruction technique	Error measure	The number of decompositions N_{part}				
		1	3	9	15	27
Averaging	SNR, dB	16.5	17.5	18.3	18.7	18.9
	MAE	0.92	0.82	0.73	0.68	0.68
Median	SNR, dB	16.5	16.9	17.7	18.5	18.8
	MAE	0.92	0.87	0.78	0.72	0.69

TABLE IV
DENOISING USING BMPT WITH PCS, $N_{\text{part}} = 9$, FOR DIFFERENT SIGNALS CORRUPTED BY GAUSSIAN NOISE ($\sigma = 3$)

Reconstruction technique	Error measure	"Doppler"	"Bumps"	"Hevisine"
Averaging	SNR, dB	14.9	15.9	19.0
	MAE	0.84	0.77	0.57
Median	SNR, dB	14.8	15.7	18.2
	MAE	0.87	0.81	0.62

Fig. 7. Original image.

Fig. 8. Image corrupted by additive Gaussian noise ($\sigma = 15$).

were calculated as the measures of efficiency of noise reduction. The SNR used is expressed as

$$\text{SNR (dB)} = 10\log_{10}\left(\frac{\sum s(i)^2}{\sum (s(i)-\hat{s}(i))^2}\right) \qquad (18)$$

where $s(i)$ denotes the true signal, and $\hat{s}(i)$ is the signal after processing.

For the 1-D case, we considered the multiresolution denoising algorithms based on the PMT [5], the MIPT [6], the BMPT, and the wavelet transform using Symmlets. The results obtained for additive white Gaussian and Laplacian noise sources are listed in Tables I and II. For all the considered algorithms of denoising, the hard thresholding scheme was used.

It is seen that the efficiency of the considered techniques depends on the noise characteristics and the signal behavior. In particular, for the "Blocks" signal, which contains edges and flat regions only, the nonlinear pyramidal algorithms are superior to the linear wavelet technique for both noise models. On the other hand, the considered wavelet-based method is more effective for the "Doppler" signal. It also follows from the tables that the median-based pyramids have smaller MAE values than the wavelet algorithms for all the signals corrupted by Laplacian noise.

Analyzing the results for the considered median-based techniques, it can be noted that the PMT is the best method in most cases under both SNR and MAE criteria. One exception is the "Bumps" signal, for which the BMPT is more effective. On the other hand, the MIPT and BMPT result in smaller sizes of transform coefficients and require fewer computations than the PMT, which is based on a dyadic structure and the sliding median operation. Therefore, the applications of one or another method can be justified from different points of view.

Obviously, the efficiency of multiscale denoising can depend significantly on the number of scale levels and on the adjustment of thresholds. With this in mind, Fig. 6 shows the plots of SNR values versus the number of scales K_0 for the four test signals

TABLE V
RESULTS OF THE "CAMERAMAN" IMAGE DENOISING USING THE BMPT AND SEVERAL TRADITIONAL FILTERS

Error measure	Noisy	Hard thr.	Soft thr.	PCS + local adapt.	Wiener (3x3)	Wiener (5x5)	Median (3x3)	Median (5x5)
SNR, dB	19.02	21.61	22.71	23.93	23.67	22.67	20.11	17.72
MAE	11.97	7.14	6.87	5.49	6.34	6.51	8.00	8.80

using the MIPT and the BMPT. The signals were corrupted by Gaussian white additive noise. The multiresolution structure of the two transforms is close to each other, and consequently, it is reasonable to compare their performance. It is evident that the BMPT is more effective than the MIPT, according to the SNR values for almost all K_0. The results of Tables I and II are also in favor of the BMPT. Moreover, the BMPT can be implemented in an easier and more efficient manner than the MIPT.

Translation-invariant denoising can significantly improve the effectiveness of noise reduction using the BMPT. The data in Table III illustrate this fact for the "Blocks" signal. The results were obtained using the PCS algorithm for several N_{part} values. The number of scale levels of the BMPT was $K_0 = 3$. Hence, the right-most column with the number of decompositions $N_{\text{part}} = 27 = 3^3$ corresponds to the full translation-invariant BMPT.

It can be seen that the effectiveness of denoising under the SNR and the MAE criteria is increasing with the growth of N_{part}. However, the most essential part of the increase exists for small values of N_{part}, indicating that the partial cycle-spinning algorithm is quite useful.

In Table IV, the results of applying the PCS algorithm with $N_{\text{part}} = 9$ are shown for different signals corrupted by Gaussian noise ($\sigma = 3$). By comparing these results with those shown in Table I, it is evident that the PCS algorithm provides significant improvement, even for small N_{part}.

As a 2-D test signal, we chose the "Cameraman" image corrupted by additive white Gaussian noise ($\sigma = 15$). The original and noisy images are depicted in Figs. 7 and 8, respectively. The results of BMPT-based denoising are presented in Table V for different thresholding schemes. In addition to simple hard and soft thresholding techniques, a hybrid scheme based on the PCS algorithm and spatial adaptive thresholding using $\eta_{\text{ad}}(\varepsilon^{(k)}; v^{(k)}; t_k)$ is presented. For comparison reasons, the results of Wiener filters as well as median filters with window sizes 3×3 and 5×5 are shown. It can be seen from Table V that the use of local adaptation and the PCS algorithm improves the effectiveness of BMPT-based denoising, according to both MAE and SNR values. In addition, the above-mentioned hybrid technique is superior to the considered Wiener and median filters. It should be noted that the advantage of this technique as compared with the Wiener filters is more evident under the MAE criterion. Although it is not shown here, the proposed method is also superior to the considered filters for Laplacian noise. Fig. 9 shows the denoised image using the PCS algorithm and spatial adaptive thresholding for Gaussian noise.

Fig. 9. Image after denoising using the PCS algorithm and spatial adaptive thresholding.

V. CONCLUSIONS

In this paper, we have proposed a block-median pyramidal transform based on nonoverlapping block decomposition. This transform is based on the median operation and linear Lagrange interpolation. Several algorithms have been proposed for denoising applications of the BMPT. Numerical simulations have indicated that these algorithms are effective for noise removal in 1-D and 2-D signals.

For the given pyramidal decomposition structure, we analytically derive the probability distribution function of the transform coefficients under the assumption of i.i.d. noise. This is used for selecting thresholds for denoising applications. The proposed structure can be implemented in an efficient manner.

ACKNOWLEDGMENT

The authors would like to express their gratitude to Dr. D. Gevorkian for useful suggestions.

REFERENCES

[1] P. Burt and E. Adelson, "The Laplacian pyramid as a compact image code," *IEEE Trans. Commun.*, vol. COMM-31, pp. 532–540, 1983.
[2] H. J. A. M. Heijmans and J. Goutsias, "Some thoughts on morphological pyramids and wavelets," in *Proc. Ninth Eur. Signal Process. Conf.*, Rhodos, Greece, 1998, pp. 133–136.
[3] R. Öktem, P. Kuosmanen, and E. Egiazarian, "Image compression using pyramidal distance order statistic filtering," in *Proc. of IEEE Digital Signal Process. Workshop*, Loen, Norway, 1996, pp. 33–36.
[4] J.-L. Starck, F. Murtagh, and A. Bijaou, "Multiresolution and astronomical image processing," in *Proc. Astron. Data Anal. Software Syst. IV*, 1995.
[5] ——, *Image Processing and Data Analysis. The Multiscale Approach.* Cambridge, U.K.: Cambridge Univ. Press, 1998.
[6] D. L. Donoho and T. P. Y. Yu, "Robust nonlinear wavelet transform based on median-interpolation," in *Conf. Rec. Thirty-First Asilomar Conf. Signals, Syst. Comput.*, vol. 1, 1997, pp. 75–79.

[7] J.-L. Starck, F. Murtagh, and M. Louys, "Astronomical image compression using the pyramidal median transform," in *Proc. Astron. Data Anal. Software Syst. IV*, 1995.
[8] R. L. de Queiroz and D. A. F. Florencio, "Pyramidal coder using a nonlinear filter bank," in *Proc. IEEE Int. Conf. Acoust., Speech Signal Process.*, vol. 3, 1996, pp. 1570–1573.
[9] A. K. Al-Asmari, "Optimum bit rate pyramid coding with low computational and memory requirements," *IEEE Trans. Circuits Syst. Video Technol.*, vol. 5, pp. 182–192, 1995.
[10] D. P. de Garrido, W. A. Pearlman, and W. A. Finamore, "A clustering algorithm for entropy constrained vector quantizer design with applications in coding image pyramids," *IEEE Trans. Circuits Syst. Video Technol.*, vol. 5, pp. 83–94, 1995.
[11] T. K. Tan, K. K. Pang, and K. N. Ngan, "A frequency scalable coding scheme employing pyramid and subband techniques," *IEEE Trans. Circuits Syst. Video Technol.*, vol. 4, pp. 203–207, 1994.
[12] F. Sattar, L. Floreby, G. Salomonsson, and B. Lovstrom, "Image enhancement based on a nonlinear multiscale method," *IEEE Trans. Image Processing*, vol. 6, pp. 888–895, 1997.
[13] P. M. B. van Roosmalen, S. J. P. Westen, R. L. Lagendijk, and J. Biemond, "Noise reduction for image sequences using an oriented pyramid threshholding technique," in *Proc. IEEE Int. Conf. Image Processing*, vol. 1, 1996, pp. 375–378.
[14] B. Aiazzi, S. Barinti, and L. Alparone, "Multiresolution adaptive filtering of signal-dependent noise based on a generalized Laplacian pyramid," in *Proc. IEEE Int. Conf. Image Processing*, vol. 1, 1997, pp. 381–384.
[15] D. L. Donoho and T. P. Y. Yu, "Nonlinear 'wavelet transform' via median-interpolation", , Tech. Rep., Stanford Univ., Stanford, CA, 1997.
[16] D. A. Florencio and R. W. Schafer, "A nonexpansive morphological pyramid image coder," in *Proc. IEEE Int. Conf. Image Processing*, vol. 2, 1994, pp. 331–335.
[17] V. Melnik, I. Shmulevich, K. Egiazarian, and J. Astola, "Iterative block-median pyramid transform-based denoising," in *Proc. SPIE Wavelet Applicat. Signal Image Process.*, vol. 3813, M. A. Unser, A. Aldroubi, and A. F. Laine, Eds., Denver, CO, 1999, pp. 502–511.
[18] R. R. Coifman and D. L. Donoho, "Wavelets and statistics," in *Translation-Invariant De-noising*. New York: Springer-Verlag, 1995, pp. 125–150.
[19] S. Marshall, D. Florencio, J. Brunt, and G. Matsopoulos, "Data cylinders in medical image fusion," in *Proc. IEEE Workshop Nonlinear Signal Image Process.*, Neos Marmaras, Greece, 1995, pp. 893–896.
[20] V. Melnik, I. Shmulevich, K. Egiazarian, and J. Astola, "Image denoising using a block-median pyramid," in *Proc. IEEE Int. Conf. Image Process.*, Kobe, Japan, 1999.
[21] G. A. Korn and T. M. Korn, *Mathematical Handbook for Scientists and Engineers, Definitions, Theorems and Formulas for Reference and Review*. New York: McGraw-Hill, 1968.
[22] I. Pitas and A. N. Venetsanopoulos, *Nonlinear Digital Filters: Principles and Applications*. Boston, MA: Kluwer, 1990.
[23] P. D. Wendt, E. J. Coyle, and N. C. J. Gallagher, "Stack filter," *IEEE Trans. Acoustics, Speech, and Signal Processing*, vol. ASSP-34, pp. 898–911, 1986.
[24] O. Yli-Harja, "Formula for the joint distribution of stack filters," *IEEE Signal Processing Lett.*, vol. 1, pp. 129–130, 1994.
[25] D. L. Donoho, "Denoising by soft thresholding," *IEEE Trans. Inform. Theory*, vol. 41, pp. 613–627, 1994.
[26] M. S. Crouse, R. D. Novak, and R. G. Baraniuk, "Statistical signal processing using wavelet-domain hidden Markov models," in *Proc. SPIE Wavelet Applicat. Signal Process. Image Process. V*, vol. 3169, San Jose, CA, 1997, pp. 248–259.
[27] S. Foucher, G. B. Benie, and J.-M. Boucher, "Unsupervised multiscale speckle filtering," in *Proc. IEEE Int. Conf. Image Process.*, vol. 1, 1996, pp. 391–394.
[28] S. G. Chang, B. Yu, and M. Vetterli, "Spatially adaptive wavelet thresholding with context modeling for image denoising," in *Proc. IEEE Int. Conf. Image Process.*, vol. 1, 1998, pp. 535–539.
[29] M. E. Zervakis, V. Sundararajan, and K. K. Parhi, "A wavelet-domain algorithm for denoising in the presence of noise outliers," in *Proc. IEEE Int. Conf. Image Process.*, vol. 1, 1997, pp. 632–635.
[30] K. Egiazarian and J. Astola, "New algorithm for removing of mixed (white and impulsive) noise from images," in *Proc. IS&T/SPIE Symp. Electron. Imaging: Sci. Technol.*, vol. 3646, San Jose, CA, 1999.
[31] J. C. Pesquet, H. Krim, and H. Carfantan, "Time-invariant orthonormal wavelet representations," *IEEE Trans. Signal Procesing*, vol. 44, pp. 1964–1970, Aug. 1996.

Vladimir P. Melnik was born in 1966 in Khmelnitsky, Ukraine. He received the M.Sc. degree in electrical engineering from the Kharkov Aviation Institute (KAI), Kharkov, Ukraine, in 1992. Since 1998, he has been with the Signal Processing Laboratory, Tampere University of Technology, Tampere, Finland, where he received the D. Tech. degree in 2000.

Between 1992 and 1998, he was a researcher and senior researcher at the same institute with the Department of Transmitting and Receiving Devices. In 1997, he received the Candidate of Technical Science degree from KAI. His research interests include image and signal processing and their applications.

Ilya Shmulevich (M'97) received the Ph.D. degree in electrical and computer engineering from Purdue University, West Lafayette, IN, in 1997.

From 1997 to 1998, he was a postdoctoral researcher at the Nijmegen Institute for Cognition and Information, University of Nijmegen and National Research Institute for Mathematics and Computer Science, University of Amsterdam, Amsterdam, The Netherlands, where he developed computational models of music perception and recognition. Presently, he is a Senior Researcher with the Tampere International Center for Signal Processing, Signal Processing Laboratory, Tampere University of Technology, Tampere, Finland. His research interests include nonlinear signal and image processing, computational learning theory, and music recognition and perception.

Karen Egiazarian (SM'96) was born in Yerevan, Armenia, in 1959. He received the M.Sc. degree in mathematics from Yerevan State University in 1981 and the Ph.D. degree in physics and mathematics from Moscow State University, Moscow, Russia, in 1986. In 1994, he received the D.Tech. degree from the Tampere University of Technology, Tampere, Finland.

He has been Senior Researcher with the Department of Digital Signal Processing, Institute of Information Problems and Automation, National Academy of Sciences of Armenia, Yerevan. Since 1996, he has been an Assistant Professor with the Signal Processing Laboratory, Tampere University of Technology, where he is currently a Professor leading the Spectral and Algebraic Methods in DSP Group. His research interests are in areas of applied mathematics, signal processing, and digital logic.

Jaakko Astola (F'00) was born in Helsinki, Finland, in 1949. He received the B.Sc., M.Sc., Licenciate, and Ph.D. degrees in mathematics from Turku University, Turku, Finland, in 1972, 1973, 1975, and 1978, respectively.

From 1976 to 1977, he was a Research Assistant with the Research Institute for Mathematical Sciences, Kyoto University, Kyoto, Japan. Between 1979 and 1987, he was with the Department of Information Technology, Lappeenranta University of Technology, Lappeenranta, Finland, holding various teaching positions in mathematics, applied mathematics, and computer science. From 1988 to 1993, he was an Associate Professor in applied mathematics with the University of Tampere (TUT), Tampere, Finland. Currently, he is a Professor of digital signal processing at TUT and the Director of the Tampere International Center for Signal Processing (TICSP). His research interests include signal processing, coding theory, and statistics.